Ingram, S., Rovelli, G., Song, Y. C., Topping, D., Dutcher, C. S., Liu, S., Nandy, L., Shiraiwa, M., & Reid, J. P. (2021). Accurate Prediction of Organic Aerosol Evaporation Using Kinetic Multilayer Modeling and the Stokes–Einstein Equation. *Journal of Physical Chemistry A*, *125*(16), 3444–3456. https://doi.org/10.1021/acs.jpca.1c00986

Accurate Prediction of Organic Aerosol Evaporation Using Kinetic Multilayer Modelling and the Stokes-Einstein Equation

Stephen Ingram,[1] Grazia Rovelli,[1] Young-Chul Song,[1] David Topping,[2] Cari S. Dutcher,[3,4] Shihao Liu,[3] Lucy Nandy,[3] Manabu Shiraiwa,[5] Jonathan P. Reid[1,*]

[1]*School of Chemistry, University of Bristol, Cantock's Close, Bristol BS8 1TS, UK*
[2]*Department of Earth and Environmental Sciences, University of Manchester, Oxford Rd, Manchester, M13 9PL, UK*
[3]*Department of Mechanical Engineering, 111 Church St SE, Minneapolis, MN, USA*
[4]*Department of Chemical Engineering and Materials Science, 421 Washington Ave. SE, Minneapolis, MN, USA*
[5]*Department of Chemistry, University of California, Irvine, CA 92697-2025, USA*

Corresponding author e-mail: j.p.reid@bristol.ac.uk

Abstract

Organic aerosol can adopt a wide range of viscosities, from liquid to glass, depending on the local humidity. In highly viscous droplets, the evaporation rates of organic components are supressed to varying degrees, yet water evaporation remains fast. Here, we examine the co-evaporation of semi-volatile organic compounds (SVOCs), along with their solvating water, from aerosol particles levitated in a humidity-controlled environment. To better replicate the composition of secondary aerosol, non-volatile organics were also present, creating a 3-component diffusion problem. Kinetic modelling reproduced the evaporation accurately when the SVOCs were assumed to obey the Stokes-Einstein relation, and water was not. Crucially, our methodology uses previously collected data to constrain the time-dependent viscosity, as well as water diffusion coefficients, allowing it to be predictive rather than postdictive. Throughout the study, evaporation rates were found to decrease as SVOCs deplete from the particle, suggesting path function type behaviour.

I. Introduction

Key transformations undergone by organic aerosol as a result of atmospheric processing remain poorly characterised.[1,2] It is important to rectify this; the ability of climate and air quality models to make predictions about the future of our atmosphere is coupled to the level of detail used to represent particulate matter in such models. At present, few dynamic phenomena are included, due to computational limitations or a lack of available parametrisations for physicochemical processes and properties. A further complicating factor is that atmospheric aerosol themselves are influenced by the meteorological conditions that they, in turn, can influence, creating a form of feedback that is challenging to predict.

Current research at the interface of climate science and aerosol science is multifaceted, because the impacts of aerosol can be wide ranging, influencing for instance cloud cover,[3,4] pollution in cities,[5] and the radiative balance of the atmosphere.[6] The incorporation of the fundamental physicochemical properties of aerosol as more accurate measurements become available, including evaporation rates, into the prediction of weather and climate, is challenging. It is important to identify instances where gaps in the current scientific understanding of aerosol microphysics limit our ability to predict atmospheric phenomena, such as those mentioned above, and focus particular attention on those areas.[7] The time-dependent proportion of the particle-phase organic material that is able to partition into the gas phase as a function of viscosity is a key parameter in predicting the evolution of secondary organic aerosol (SOA). Consider a three step process: Firstly, the volatility of an organic species is reduced as it is oxidised in the atmosphere, forming a semi-volatile organic compound (SVOC).[2,8] Next, the molecule partitions into an existing aerosol SOA particle, or nucleates a new particle, and becomes solvated by a condensed phase matrix. Finally, chemical reactions, or changes in the local atmospheric conditions, promote the re-evaporation of the species. The rate of this evaporation is strongly influenced by the viscosity of the surrounding particle matrix, as any molecule must first diffuse to the surface before it can evaporate.[9]

At present, the extent to which molecular diffusion within aerosol particles is slowed by a given increase in viscosity is the subject of some debate: different experimental techniques disagree about the limiting value of diffusion coefficients as a particle approaches a glassy state.[10–12] Indeed, diffusion in ternary-component mixtures is a challenging problem in chemical physics more broadly and has been little explored in the current literature, wholly separate even from its utility in understanding the evaporation of SOA from aerosol in the atmosphere.[13] However, especially at the solute concentrations accessed in organic aerosol, molecular diffusion becomes complex and highly sensitive to slight changes in solubility or intermolecular interactions.

Often, a complex array of chemical and physical processes can be approximated by a simpler, heuristic quantity. For instance, one can represent the oxidation state of ambient organic aerosol using the mean oxygen to carbon (O:C) ratio of the organic constituents. As a particle is aged by the gas-phase species it encounters, the organic backbones of the constituent molecules are gradually functionalised with C-O, C-OO or C=O bonds, and the ratio approaches (or exceeds) 1. Generally, larger and more highly oxidised

molecules possess higher pure component viscosities,[14,15] leading to a significant disequilibria developing in composition between the interior of the particles and the gas phase. Processes such as diffusion or further oxidation are then slowed to an increasing extent. Decreasing vapour pressure[16] or changing cloud nucleation ability[17] are exhibited by the particles as they are processed by the atmosphere.

While a complete representation of the chemistry and microphysics occurring in viscous aerosol would be too computationally expensive to explicitly represent in large-scale models, very few regional or global climate models currently include any representation of gas-particle disequilibria. One possible method to capture such effects may be to use structure activity relationships, which seek to find empirical correlations by amassing large amounts of experimental data.[15] Indeed, O:C ratio is the only metric which large scale atmospheric models use to represent aerosol composition. Other complicating factors are the strong influences of moisture[18–20] and temperature,[21] in addition to environmental processing, on particle viscosity.

Perhaps the most recognised relationship between viscosity and diffusion is the Stokes-Einstein equation:

$$D = \frac{kT}{6\pi\eta a} \qquad 1$$

which equates the diffusion coefficient of a species, *D*, to the ratio of the thermal energy, *kT*, supplied by the surroundings, to the friction that that species experiences (via Stokes' Law). η is the dynamic viscosity and a is the molecular radius.

It has been known for some time that the relationship between viscosity and diffusion reflected in the SE equation is not universally applicable, i.e. under certain conditions it fails, and the macroscopic viscosity η no longer predicts the microscopic diffusion *D*. This 'breakdown' has been observed to occur in various chemical systems, such as those containing a high degree of hydrogen bonding,[22] polymeric substances,[23] those undergoing supercooling,[24–26] those exhibiting confinement of small molecules within porous networks,[27] or in systems which are close to undergoing a glass transition.[26,28] Strikingly, the internal structuring of a tropospheric organic particle is thought likely to depend on every one of these factors.[29–32] It is therefore not surprising that the SE equation routinely fails to predict the observed relationship between diffusivity and viscosity in different types of SOA. Indeed, in our previous publication[33] we proposed to directly link the nanoconfinement of water to the failure of Stokes' Law, by invoking a new mechanism of water transport, that proceeds via hopping between discrete sites. In addition, there is evidence that significant heterogeneities exist in the concentration and rotational motion of organics in particles from fluorescence imaging studies.[34] Such 'dynamic heterogeneity' may be significant enough to influence the mean diffusion rate, averaged over the droplet. More generally, it is a common feature of molecular glasses,[35] whose dynamics are known to be inconsistent with Stokes' Law.

On the other hand, many publications within the aerosol science field report exclusively on the failure of the SE equation to describe the diffusion of water and other small, polar molecules. In the context of the

atmospheric literature, there is an emerging consensus that water transport remains 'fast' (particle mixing times <1 hr) under most conditions, at least in the planetary boundary layer.[36,37] This has been corroborated recently by observations of aerosol sampled from both urban[38] and rural[39] sites. However, the diffusion of organic species in viscous multicomponent aerosol, and the extent to which the Stokes-Einstein equation can represent transport, remains a focus of research.[40] On a molecular level, organic compounds tend to be larger than the solvent through which they move and this promotes Brownian trajectories which are broadly consistent with the derivation of Stokes' Law. Further, time dependent changes in the molar ratio of different organic species as they evaporate can alter the overall composition and particle viscosity. Yli-Juuti et. al.[41] recently studied the evaporation of α-Pinene SOA in a batch operated smog chamber. They found that, for the evaporation rate to be accurately modelled, a viscosity increase of at least three orders of magnitude in the early seconds of the experiment needed to be assumed.

Building upon an extensive library of laboratory data we have accumulated on binary water-organic aerosol droplet viscosities,[42] we consider here the complex behaviour of ternary mixtures containing two organic solutes. In all measurements discussed here, the most concentrated solute by mass is always a high molecular weight viscous sugar. The sugars are intended to replicate the physical and chemical properties of highly oxidised[8] or oligomeric[31] constituents of aged SOA. Also present in the droplets are semi-volatile organic solutes, chosen such that they will slowly evaporate, along with their solvating water. As in our previous studies,[10,33,43] ambient humidity is controlled, influencing particle viscosity, which in turn affects the timescale of evaporation.

We discuss and implement two methods to predict three component particle viscosity in situations where the ratio of non-volatile to semi-volatile components is changing. We find that the evaporation rate, and hence diffusion rate, of the SVOCs from SOA can be predicted accurately using Equation 1, without any of the modifications[44] or fractional terms[28] that are occasionally discussed in the literature.[45,46] This appears a general trend, i.e. not dependent on the initial volatility of the SVOC, since the two investigated here (glycerol and malonic acid) possess vapour pressures that differ by approximately a factor of 20. More precisely, we can say that this holds across all studied humidities (25 – 75%, at room temperature), assuming a rigorous parametrisation of ternary composition is included within the kinetic model. We will describe the parametrisations further in section III, before comparing the experimental data with the model predictions in section IV.

II. Methods

The experiments discussed herein were conducted on individual droplets using a combination of optical and electrodynamic trapping methods. As most of the data were acquired using optical tweezers, this technique will be introduced first. These techniques have been described extensively in previous publications[47] and only a brief summary will be provided here.

II.a Aerosol Optical Tweezers (AOT)

A small volume of solution is prepared and loaded into an Omron U22 MicroAIR nebuliser. The aerosolised plume of solution then flows across a focused 532nm wavelength laser until one of the particles strays close to the focal point and becomes trapped by the optical forces. Once this occurs (as observed by brightfield imaging), the nebulisation is ceased, and the particle is isolated from the laboratory atmosphere. It is then exposed to a nitrogen gas flow of controlled humidity. Some droplets are captured directly at the humidity under consideration, whereas others are dried consecutively and evaporated multiple times.

Once a droplet is trapped, or following to a step-change in relative humidity, the water activity in the particle is allowed to equilibrate with the water content in the gas phase, after which point the dominant process controlling mass loss is the evaporation of the semi-volatile dicarboxylic acid or alcohol.[10,48] Here, the radius decrease rather than mass loss is inferred, as determined by the cavity enhanced Raman signature from the droplet. Within the Raman scattering spectral range, Mie scattering occurs within the interior of the particle, leading to enhanced resonances at wavelengths that shift in accordance with circumference, and hence radius. The Mie theory differential equations are solved via a core-shell fitting program (more details provided in the supplement), producing estimates of refractive index in addition to radius. These estimates are refined to produce the radius data shown in section IV.

II.b Electrodynamic Balance

Electrodynamic trapping is also used to levitate particles in this study. As detailed in previous publication,[49] single charged droplets can be generated from an initial solution with desired chemical composition by using a droplet on-demand dispenser (Microfab MJ-ABP-01). Accessible droplet radii with this experimental setup range from to 4 to ~30 μm, which contrasts with 3 – 7 μm for the optical tweezer apparatus. Once dispensed, a single droplet is delivered to the centre of the electrodynamic field generated by a set of concentric cylindrical electrodes, which allows indefinite levitation of the droplet within a nitrogen flow with controlled temperature and relative humidity (in this study T = 293 K, RH from 0 to 90%). In addition, a 532 nm wavelength laser illuminates the trapped droplet; the elastic light scattering arising from it is collected with a camera (Thorlabs CMOS camera, DCC1545M) and used to infer the droplet evolving size by applying the geometric optics approximation.[50]

II.c Identifying a Bulk-Diffusion Limitation on Evaporation

By using our previously employed methodology, based on the Maxwell treatment of evaporation,[10] it is possible to determine the partial pressure of semi-volatile compounds p_{svoc} above the surface of a levitated droplet from the recession of its radius, either from the optical tweezers or electrodynamic trapping measurements. In the case that there is no kinetic impairment from high viscosity on the rate of evaporation, the value of p_{svoc} would increase with the surface concentration of solute as the droplet dries.

$$p_{svoc} = x_{svoc} \cdot \gamma_{svoc} \cdot {p_{svoc}}^{\ominus} \qquad 2$$

Any deviations from this Raoult's law type behaviour can be attributed to a kinetic slowing of the resupply of the evaporating species to the particle interface. It therefore follows that, if the mole fractions x_{svoc} and activity coefficients γ_{svoc} are accurately known across the RH range of the experiments, the pure component vapour pressure, ${p_{svoc}}^{\ominus}$, can be calculated for each particle at each potential RH. The humidity at which a reduction in the value is observed will indicate the onset of the bulk diffusion limited regime. Throughout this paper we refer to the reduced values of ${p_{svoc}}^{\ominus}$ calculated as the effective pure component vapour pressure, or effective vapour pressure.

A complicating factor we wish to investigate is the path dependence observed in the evaporation of viscous organic droplets. That is to say, the fact that the humidity that a particle currently experiences does not fully determine the rate of evaporation. In fact, the entire processing history of a particle since its formation must be considered to fully understand the influence of viscosity and particle phase concentration on the loss of semi-volatile species.[43] If there is an influence of semi-volatile depletion on the observed evaporation rate, then comparisons of particles experiencing the same RH, but with different drying trajectories, will reveal it.

III. Kinetic Modelling

Here we use a modified version of the KM-GAP model, first described by Shiraiwa et. al.[51] to forward simulate the portion of the experiment where organic evaporation dominates, following the initial equilibration in water content between the particle and gas phases. It has been observed in several studies[41,52] that the microphysical treatment of particle phase diffusion employed is crucially important to accurately model the evaporation data. In contrast to the Monte-Carlo-Genetic-Algorithm procedure that is usually applied in KM-GAP,[53] whereby multiple diffusion constants are varied in order to optimize the model output to the data, here we have fixed diffusion constants according to independent viscosity measurements. The organic compounds have been assumed to follow the Stokes-Einstein relation, with η determined through aerosol coalescence and shape relaxation measurements across the range of relative humidities for single solute systems.[42]

The viscosity of a ternary mixture is parametrised from the constituent solutes using mixing rules that will be the subject of the detailed discussion in section IV.a. Once a parametrisation of η has been produced, we can convert it to a diffusion constant for the organic compounds via the SE relation (Equation 1). The Stokes radii used were calculated from the volume of a single molecule at the pure melt density[54], and are as follows: 8.2 Å for raffinose, 7.2 Å for sucrose, 5.0 Å for glycerol and 4.7 Å for malonic acid. Additionally, we model water transport using the sigmoidal dependence of its diffusion coefficient on water mole fraction determined in our methodology paper.[10]

The resulting relations between diffusion coefficients and relative humidity for each component in a water-raffinose-malonic acid ternary mixture are shown in Figure 1. As predicted, the organic molecules diffuse between two and four orders of magnitude slower than water, with the ratio widening towards the lower end

of the RH range presented. The 'curvature' of the two organic parametrisations in log-space are identical, as they only differ by a constant factor. The absence of a bulk diffusional limit on organic and water transport at high moisture content diminishes the sensitivity of the model to the parameterisation of all of the diffusional constants at high limiting RH, particularly above ~75 % RH; we do not consider this high RH regime here.

Another modification to the KM-GAP model is the introduction of Raoult's law (Equation 2) to correct the equilibrium partial vapour pressure of the semi-volatile component according to the surface mole fraction. This is updated at every time step that the model is evaluated, to capture the time evolving nature of the droplet chemical composition and, therefore, its volatilisation. The length of the input model timesteps is varied over the course of one simulation: the solution of the differential equations governing diffusion is calculated for a 1000 element time vector that increases logarithmically from 0.1 s to the length of the experiment (range 5000–35,000 s).

When comparing predicted to observed radius data, other model details are as follows: the particle density has been calculated from the experimental RH using polynomial dependencies published previously[54] for the relevant binary aqueous-solute systems along with an assumption of ideal mixing when calculating the density of a complex mixture. Where available, the starting mole fractions and activity coefficients of the various organic species and water have been determined by employing the statistical thermodynamic treatment of Dutcher et. al.[55–57] Their values are presented as a function of water activity in Figures S1 and S2. Other model parameters and modifications are also provided in the supplement.

IV. Results and Discussion

IV.a Estimation of the viscosity of two solute systems based on hygroscopic growth

While it is possible to determine the viscosity of simple, one solute systems in the aerosol phase, or of SOA particles, systems of intermediate complexity represent a challenge. If data are not available, we require a methodology to predict the viscosity of a mixture from its constituent parts. Ternary aerosol therefore represents a stepping stone between binary systems, the viscosity of which can be inferred from reliable and reproducible measurements,[42,58] and the incredibly complex task of probing atmospheric aerosol in the natural environment. Indeed, a methodology is required that can accurately predict the viscosity of a mixture if the constituent molecules and their molar ratios are known. We discuss below the method used to predict particle viscosity in situations where the ratio of non-volatile to semi-volatile components is changing over time, due to the volatilisation of one of the organic components and water.

A group contribution based method for the prediction of multicomponent aerosol viscosity was published recently by Gervasi et al.[59], which has shown remarkable accuracy, suggesting this may become an active area of research. In the present work, we implemented the approach described by Rovelli et al., weighting the viscosity contributions from each species present in each particle according to its hygroscopic properties.[60] Conversely, when considering time dependent changes in viscosity as plasticising organic

molecules become depleted from the particle, a simpler mole fraction mixing rule is found to provide a sufficient level of detail. Both kinds of dependence can be considered types of the so-called Bosse mixing rule. The procedure involves a sum over the logarithms of the pure component viscosities of each component *i*:

$$\ln(\eta_{mixture}(a_w)) = \sum_{i}^{n} x_i \ln(\eta_i(a_w)) \quad 3$$

where each compound is weighted by its mole fraction x_i. Here, the hygroscopic growth of each solute is considered separately, allowing the water mass present to be divided between the two. Each pure component viscosity is replaced with the binary mixture viscosity of i and water, at a recalculated water activity, $\eta_i(a_{w,i})$.

It is assumed that each solute does not influence the association of water to other solutes. Therefore, the local environment of either solute within the droplet is considered to be a binary solution with a separate water activity to the other. Each new $a_{w,i}$ value for a solute i is calculated using partial mass fractions of water, $m_{H_2O,i}$, taken from the hygroscopic growth factor measurements of the relevant binary solution aerosol, as discussed in reference 60.

Several examples of mixing rules for viscosity in three component aerosol are shown in Figure 2. Panel (a) presents the viscosities of raffinose and glutaric acid measured in our previous publication (purple and yellow respectively).[42] A simple mole fraction based mixing rule prediction for a droplet prepared with a 3:2 molar ratio of non-volatile to semi-volatile is shown in green. To illustrate the sensitivity of the viscosity to composition, the viscosity is also shown following a 90% depletion of the glutaric acid component from a hypothetical particle (green dashed line), a highly vitrified case. The difference in magnitude caused by such a change in composition is significant, and will be of crucial importance when interpreting the experiments described in section IV.c.

In Figure 2 we also present the application of equation 3 to predictions of the viscosities of a 1:1 molar mixture of glycerol and sucrose. Panel (b) contains a static representation of the mixture viscosity as a function of dehydration, alongside the binary solute parametrisations for the semi-volatile and nonvolatile species, showing similar trends to panel (a). Glycerol is a semi-volatile molecule with a low molecular weight, and so does not achieve a glassy state under dry conditions (black line), in contrast to sucrose (green). The vertical line represents the humidity at which the evaporation experiment interpreted in a later subsection (IV.c) was conducted. Panel (c) presents three time dependent viscosities estimated from evaporation measurements using the EDB for the same system for three single droplet measurements starting with initial molar ratio of 1:1 glycerol:sucrose at three different RHs. As glycerol evaporates from each ternary droplet, the droplets becomes increasingly rich in sucrose and the viscosity increases in time. The viscosity shown in Figure 2c is estimated using the mixing rule described above based on radius changes measured at three fixed RHs, 70, 60 and 25%. The evolving concentrations of water, glycerol and sucrose

were estimated from their initial concentration and the measured particle volume change. Data were averaged over logarithmic time bins and the larger uncertainty observed for the lowest RH experiment reflects the uncertainty on the sizing of this particular droplet. In all three cases, we observe two entirely separate timescales where the viscosity of the droplets increases. The first, from 1-10 s, is caused by the loss of water from the droplet during equilibration with the RH. The second, from 10^3-10^5 s, is caused by the much slower evaporation of glycerol.

IV.b Predictions of kinetically limited evaporation

As a result of the resupply of the humidified nitrogen gas flow within the trapping cell, there is no saturation of semi-volatiles within the immediate atmosphere of the levitated droplets in this study. This maintains a continuous thermodynamic driving force for evaporation and the particle-phase concentration of any semi-volatiles monotonically decreases over time. Thus, an upper limit of the mass flux due to volatilisation can be determined as a function of the pure component vapour pressure:

$$\frac{dm}{dt} = \frac{4\pi M_{svoc} D_{gas}}{RT}(p_{svoc}) \quad (4)$$

where M_{svoc} is the molecular mass of the evaporating species in Kg and D_{gas} is its gas diffusion constant in m^2s^{-1}. R is the gas constant and T is the temperature in K. As an example, assuming a 4.5 μm droplet composed entirely of a single semi-volatile species whose properties are $p_{svoc} = 10^{-3}$ Pa and $M_{svoc} = 100$ g mol^{-1}, and with no kinetic limitation, the above equation predicts that approximately 14% of the droplet mass will be lost per hour.

In a ternary mixture, as discussed in the previous section, viscosity increases by many orders of magnitude as the concentration of water approaches zero, i.e. as the relative humidity is reduced and as the SVOC is lost from the particle. This has the effect of kinetically limiting the resupply of semi-volatiles to the surface and quenching the mass loss. We have shown this in Figure 3 by comparing radius data extracted from the Raman signals of optically levitated raffinose (involatile) + malonic acid (semi-volatile) particles in different RH environments. As the humidity decreases, the rate of evaporation also decreases. While the surface concentration of organics is higher at 45% compared to 68% RH, in both cases this layer will be enriched in the involatile species after a few minutes of exposure to the N_2 flow. If the initial viscosity is high enough then, once the outermost few nanometers of the particle are depleted of malonic acid, the surface becomes a 'crust' that increasingly traps the remaining SVOC molecules in the particle bulk.[61]

Under the gas diffusion limited regime, by contrast, the radial concentration profile within the particle remains flat as the concentration of semi-volatiles decreases, and any molecule can diffuse from the particle centre to the surface without impediment.[52] In that case the above equation (#4) will provide an estimate of the amount of semi-volatile species that may be depleted during each period the droplet is held at a constant RH. A more thorough discussion of what is occurring internally in particles with multiple chemical systems will be presented in section IV.c. For now, it is the transition between these two regimes that is most central to our discussion.

To illustrate the effect of particle water content on the evaporation regime for an organic component, we constructed a model system to simulate the behaviour of SOA using KM-GAP. Hypothetical particles of radius 200 nm were initialised at different RHs and allowed to evaporate. This small size provided us with evaporation rate data of more relevance to the sizes of tropospheric aerosol particles. The particles were modelled to contain water and two organic solutes, with the starting composition defined such that the organic matter is 25% by volume semi-volatile, 75% non-volatile. The densities of the organic components have been fixed at 1.5 g cm^{-3} and the viscosity of the particle assumed to be the same as SOA formed from the oxidation of Toluene.[14,19] The hygroscopic growth of the particle has been included and was represented using the κ-Kohler representation,[62] according to which the changing volume of water within the droplet, V_{water}, can be represented by the equation

$$\kappa = \frac{V_{water}}{V_{dry}}\left(\frac{1}{a_w} - 1\right) \quad (5)$$

where a_w is the particle phase water activity. κ values of 0.1 and 0.25 were chosen for this simulation. These values are consistent with a recent parametrisation of toluene SOA hygroscopicity by DeRieux et al.,[14] who found that $0.2 < \kappa < 0.25$ could be assumed. While κ is generally considered to be dependent on RH,[63] we have used fixed values as this modelling is intended as a sensitivity study i.e. we wish to calculate an envelope bounded by the two extreme cases of κ, within which most SOA particles can be considered to reside.

The mean evaporation rate from the model, $\frac{dr^2}{dt}$, was then calculated from the radius responses across the humidity range from 100-0%, in increments of 4% RH. Instead of representing this rate as an effective vapour pressure, we more accurately relate the semi-volatile flux directly to the mass loading of vapour immediately above the surface of the particle. This is achieved by substituting the definition of mass concentration into the Maxwell treatment of the vapour pressure at a receding particle surface, producing:

$$fC^* = \frac{dr^2}{dt} \cdot \frac{\rho_{droplet} F_{svoc} \gamma}{2D_{gas}} \quad (6)$$

Where $\rho_{droplet}$ is the density of the particle and *fC* is an *effective* (or *fractional*) C*, that is linearly related to the effective vapour pressure above the surface. F_{svoc} is the mole fraction and γ the activity coefficient of the semi-volatile organic compound under consideration, and D_{gas} is as defined in equation 4. We have assumed ideality in this modelling, meaning that all compounds have a γ value of 1. Equation 6 is simply a conversion of p_{svoc} into the units of mass concentration and so the above equation is analogous to the vapour pressure equation described in our previous works.[9,10] In this way, the switch from gas phase to particle phase diffusion limited evaporation[52] can be assessed quantitatively, and represented as a change in the effective saturation of the organic components.

Six curves of the fractional *fC*(RH)* are reported in Figure 4. Recall that the absolute value of *fC** is an estimate of the saturation concentration established directly above the droplets surface as it recedes. In this

case the intrinsic saturation mass concentrations of the evaporating compounds were set to 100, 10, and 1 μg m^{-3}, i.e. we consider them as representative of three adjacent bins of a volatility basis set (VBS). A VBS is a common method used in the literature to represent the evaporation of highly complex particles by producing a histogram of component concentrations in logarithmic bins.[41] We are therefore charting how the observed volatility of each compound can deviate from its pure component value and how it may 'end up' in different bins as the particle vitrifies. As described earlier, each compound was simulated twice, assuming two different values of κ.

The evaporation rate of all three compound was found to be significantly restricted by the vitrification of the particle below an RH of approximately 50%. At both κ values (purple and orange lines), the compound with an equilibrium C* of 100 μg m^{-3} crossed into an adjacent 'volatility bin' in a more humid environment than the 10 μg m^{-3} compound, which in turn crossed over before the 1 μg m^{-3} compound. Therefore, we can say that the onset of a bulk diffusion limitation will become apparent earlier (if one starts at 100% humidity and dehydrates) in the evaporation rate of organics possessing a higher saturation concentration C*.

It was initially expected that the suppressed evaporation rates of the compounds would each be unique as a function of RH. However, this is not observed. In fact, the trend in mass loading of all compounds at a given κ value collapses onto one dependence at around 30% RH. This suggests that, once an SOA particle achieves a certain viscosity, the diffusive limitation is so severe that the evaporation rate ceases to be dependent on the inherent volatility of the organics evaporating: the partial pressure of an organic species above the surface of a sufficiently viscous particle will be suppressed proportionally to how volatile it is at equilibrium. Therefore, if volatility is measured by $\frac{dr^2}{dt}$, all organic compounds will appear to reside in the same volatility bin, regardless of their saturation concentration. It should be noted that we have not accounted for changes in the density and molecular cross section of different volatility species, which may also influence the diffusional flux in a way that separates out the different curves. However, all other parameters being equal, the statements above hold, and viscosity can be considered the primary determinant of evaporation rate at low RH.

When the assumed hygroscopicity is low (the $\kappa = 0.1$ case), the transition between the gas and bulk diffusion limited regimes occurs near the point at which the viscosity reaches 10^4 Pa s. This is within the range commonly described as 'semi-solid' in the literature (see, for example, references 14,15,21). While the viscosity required to limit bulk diffusion is dependent on the particle size, this modelling suggests that, at least for the smallest SOA particles, the onset of slow evaporation occurs well below the viscosities accessed in the glassy state. This result is significant as, in reality, SOA particles contain an array of organic solutes that can plasticise (reduce the viscosity of) their surface shells, even at low RHs.

IV.c Observations of kinetically limited evaporation

We now explore the path function dependent behaviour observed in the evaporation of viscous organic droplets in the high viscosity, slow diffusion regime. By path function behaviour we mean any situation in which the humidity that a particle currently experiences does not fully determine the rate of evaporation. Instead, the entire processing history of a particle since its formation must be considered to fully understand the viscosity and particle phase concentration of semi-volatile species.[43] If there is an influence of semi-volatile depletion on the observed evaporation rate, then comparisons of particles experiencing the same RH, but with different drying trajectories, will reveal it.

More specifically, we consider two different ternary systems. Measurements of the evaporation of malonic acid have been made from aqueous-malonic acid-raffinose particles with optical tweezers at 14 RHs, between 75 and 38%, each of which remained constant through the experiment. The lower humidity bound probed by these measurements is close to the glass transition humidity of the saccharide, meaning the potential viscosities achieved by the particles ranged from semi-solid to approaching glassy (see Figure 2). As a second system, a particle containing a large volume of glycerol was trapped in an electrodynamic balance at a constant RH of 25%, and its evaporation through an aqueous-glycerol-sucrose matrix was observed over the course of several days.

Here we aim to accurately predict changes in the particle radii during these evaporation events and consequently to quantify the influence of varying the water activity in the gas phase on the internal dynamics within the particles. The pure component vapour pressures of the semi-volatiles employed are approximately 10^{-2} and 4.3×10^{-4} Pa for glycerol and malonic acid,[64] respectively, roughly corresponding to C^* values from 20 to 160 μgm^{-3}. We consider the two systems separately.

Malonic acid evaporation from aqueous-raffinose particles

In Figure 5 we report effective pure component vapour pressures measured for raffinose-malonic acid particles. Unlike Figure 4, we choose here to explicitly to represent the change in apparent volatility with moisture content by an effective vapour pressure reported in Pa. The measurements are bounded by an envelope produced by the KM-GAP model for different limits of the starting concentration. Raffinose is a trisaccharide with a large molecular mass and, as such, raffinose particles should increase in viscosity strongly with decrease in RH.[42] The modelling confirms this more rigorously, as a steep gradient of the effective vapour pressure, p_{svoc}, versus RH is predicted in the regime where particles experience bulk diffusion limited evaporation. In contrast to the effective C^* values we used to chart changes in individual VBS bins in Figure 3, p_{svoc} is estimated from the measurements using the Maxwell treatment of a receding particle surface:

$$\frac{dr^2}{dt} = \frac{2M_{svoc}D_{gas}}{RT\rho_{droplet}F_{svoc}}(p_{svoc}). \qquad 7$$

Here, F_{svoc} is the mass fraction of the evaporating species, and all other parameters are as defined in equations 4 and 6. The relationship between equations 4 and 7 can be found in the supplement to our

previous publication.[10] The upper and lower bounds are calculated from the KM-GAP model, accounting for the interplay of a gas diffusive limitation at high RH and a condensed phase diffusive limitation as the RH is lowered, as described above, as discussed for Figure 4.

In the optical tweezers experiments, the solution was prepared with a 3:2 molar ratio of the sugar to the acid. It should be expected that almost all the malonic acid would evaporate within 3 hours of aerosolisation if the viscosity remained sufficiently low, based on an estimation using equation 4 (assuming a 4.5 μm radius particle, of density 1.5 gcm^{-3}, at 300 K). The modelling confirms this more rigorously, with the 90% relative depletion bound (i.e. a 24:1 molar ratio) encapsulating the data in the figure. The associated change in the particle viscosity based on this compositional change/depletion has already been presented and discussed in Figure 2a. Readers interested in the sensitivities of the model to these kinds of effects are directed to the supplement where we have provided intermediate contours modelled for 30 and 60% depletion (Figure S3a), as well as the influence of the uncertainty in viscosity on the predicted vapour pressure (Figure S3b).

Returning to the experimentally determined effective vapour pressures, they vary by just over a factor of ten between the highest and lowest humidities. Meanwhile, we can infer from Figure 2a that a binary raffinose/water particle would increase in viscosity by seven orders of magnitude. This discrepancy between the magnitudes by which the viscosities and evaporation rates change may be due to a rapid surface enrichment of raffinose, leading to a high surface viscosity that is not plasticised by malonic acid even at high RHs. This would not be detectable by our coalescence technique of measuring aerosol viscosity,[42] on which the model inputs are based, as the value extracted is an average over the entire volume of the particle.

Note that, at high RH, both the data and model converge to the pure component value of the vapour pressure for malonic acid in the absence of a bulk condensed phase kinetic limitation to its volatilisation. The variance in observed values of p_{svoc} is also noticeable. In our methodology paper,[10] we used refractive index as a proxy for droplet composition and proposed that increasingly saccharide rich particles would evaporate more slowly at the same RH. Here, we have used KM-GAP to directly understand the enrichment of raffinose as a function of the conditioning each particle has experienced.

As discussed in the introduction, water in viscous aerosol diffuses faster than the Stokes-Einstein relation predicts, sometimes by many orders of magnitude.[10,11] The evaporative dynamics of the particles under consideration in the present study reflects fast water diffusion occurring *in concert* with slow diffusion of organics. We have found that there is a range of intermediate humidities in which markedly different internal concentration profiles are observed for the two volatile species during the same experiment. Figure 6 presents the clearest example of this phenomenon. The loss of malonic acid from a raffinose particle at 53% RH was observed over nearly two hours in the AOT (panel (a), orange points). Subsequently, the same experiment was simulated by KM-GAP (blue line), showing very good agreement between the measured and simulated change in radius over time. It is important to appreciate that there is no fitting in this comparison

but simply a forward simulation for the ternary system. The starting radius for the simulation was chosen as the approximate moment the particle equilibrated with the ambient RH, determined by the abrupt change in the experimental evaporation rate, observable when the radius data is presented on a log time scale. Diffusion coefficients for the three components were calculated according to water activity as presented in Figure 1 and described in sections III and IV.a.

Differences in the bulk concentration profiles of the water and malonic acid depletions were calculated from the model by normalising the concentrations of both within each shell to their initial values at t = 0. The resultant matrices varied between 1 and 0 as a function of radial coordinate and time, which we present as colour maps in Figure 6b and 6c. Water loss (panel (b)) was found to be rapid, occurring from everywhere in the particle at once, while a gradient was quickly established in the concentration of malonic acid between the surface and the centre (panel (c)). This observation is remarkable given that the water volatilisation in the experiment takes place at a constant particle phase a_w – meaning that we can assume it is a co-evaporative process caused by the loss of malonic acid with a commensurate amount of solvating water. A similar trend in internal dynamics was observed at humidities as low as 20% when the saccharide present was sucrose (see Figure S4), albeit with less close agreement between the predicted and observed radii. In effect, water transport throughout the particle is rapid, responding to changes in SVOC concentration more rapidly than the SVOC itself volatilises. By contrast, there is considerable heterogeneity in SVOC concentration throughout the particle, with a depletion near the surface kinetically impeding the transport of malonic acid to the surface and volatilisation.

A second example of water diffusion producing an intraparticle concentration profile distinct from that of malonic acid was observed is at 45% RH, presented in Figure 7 in the same format as Figure 6. The initial ratio of malonic acid to raffinose at t = 0 was just over 10% depleted from the starting solution. This was determined by simulating exposure to the ambient conditions experienced by the particle immediately before the experiment began: 77% RH for 5000 s. The total radius change is very small, only 6 nm over approximately 6000 s. Clearly, at a humidity so close to the moisture driven glass transition of the saccharide (40%), water loss will be exceptionally small (only 1% of the initial value, shown in the colour scale of panel (b)). Similarly, the concentration gradient of malonic acid is found to be much more steep in the near-surface region than in the 53% RH case, with loss localised only to the surface layer (panel (c)). If these simulations are accurate in reflecting the true internal structures of the droplets, it would mean that a surface depletion of a compound can cause a “sympathetic” co-evaporation of solvating water from regions within aerosol particles far from the surface and experiencing no depletion. We hesitate to confidently assert the mechanism by which this occurs, although the cavity hopping process we described recently[33] may play a role.

Another key result of this study is that it is possible to improve the accuracy of the radius predictions by tracking the effects of multiple experiments conducted on the same particle consecutively. The approach we have adopted is as follows: the mole fractions of the two organics are output at the final timestep of each simulation as a normalised ratio, excluding water. For example, a ratio of 0.7:0.3 would be generated if one

quarter of the malonic acid had evaporated from the particle. When the humidity is stepped down to begin the next experiment, a new viscosity is then calculated: Using the Bosse mixing rule (equation 3), the output ratio is multiplied by parameterisations of prototypical involatile and semi-volatile compounds, η_1 and η_2. As before, the water content of the particle is determined from the model of Dutcher et al.[56] at the new RH, and total organic content is scaled accordingly.

Glycerol evaporation from an aqueous-sucrose particle

Next, we attempted to simulate the EDB data for glycerol evaporation, which is about 25 times more volatile than malonic acid. Despite the increased volatility, the experiments are performed over a similar timeframe to the malonic acid measurements, partly a consequence of measurements on much larger particles than with optical tweezers, but also indicating the extent of the bulk diffusive kinetic limitation imposed even for this system.

The experimental data are reported in Figure 8a, showing that the interface recedes by several hundred nanometers over the course of 30,000 s. The droplet was dispensed from a solution prepared at a molar ratio of 1:1 sucrose:glycerol, and the evaporation takes place at 25% RH. The data has a pronounced curvature, and appears exponential, or perhaps stretched exponential,[10] in nature, reflecting a second order phenomenon whereby the flux itself changes in a time dependent manner. It was decided that a time dependent viscosity parametrisation was the most appropriate way to model the changes in composition throughout the experiment. It was found that the ternary viscosity prediction for 25% RH, as presented in Figure 2c (blue points), was not appropriate to insert directly into the kinetic modelling: it is not a smooth or monotonically increasing function of time. A number of functional forms were used, but it was found that a bi-exponential function reproduced the shape of the parametrisations most accurately. We should note here that this representation lacks radial resolution – that is to say, viscosity is assumed to be the same everywhere in the particle at each timestep.

Practically, we would like to predict the timescale over which evaporation takes place, rather than its precise thermodynamic end point. For this reason, our previous publications[10,43] have converted radius data into response functions before interpreting them, as this allows a comparison to be made between model and experiment without needing to define the precise thermodynamic end point of the evaporation, among other quantities. The experimental data have regular gaps in time where no radii are reported, a result of the geometric optics approximation applied for sizing this droplet (as described in the supplement) in the electrodynamic balance,[49] which causes perturbations in the extracted radius whenever the number of recorded peaks changes. This is not believed to impact the accuracy of the fit of any of the orange points in Figure 8a.

The time dependent particle viscosity was estimated using equation 3, and is presented in panel (b) (orange points). Since the $\eta_{mixture}(t)$ calculation is dependent on the particle's volume and refractive index, there

are numerical instabilities in the solution arising from the measurement of its optical properties, as discussed above. Therefore, direct insertion of the raw viscosity data into KM-GAP resulted in the ODE stiffening each time a step change was encountered. It was found that a lower resolution, smoothly varying function had to be used instead. Of the functions tried, it was found that a bi-exponential dependence on time (yellow line) best reproduced the shape of the mixing rule prediction. Further details are provided in the supplement.

The KM-GAP radius change underpredicts and overpredicts the experimental data by tens of nanometers at different points in time (blue line, figure 8 panel (a)), but generally captures the magnitude of the evaporation. Additionally, both the initial gradient and the aforementioned 'folding' time as the glycerol is depleted from the particle, are reproduced accurately. We reiterate that these simulations only rely on information that has been determined experimentally, namely the starting radius and the compositional dependence of the viscosity of the system, in this case estimated from water-activity dependent single component measurements. The success or failure of the approach, then, relies on the validity of the assumptions inherent to the model rather than fitting and optimisation of the parameter space.

The internal concentration gradients of water and glycerol produced by the model (panels (c) and (d) respectively) suggest a relatively balanced contribution of each to the overall evaporation. Unlike in the malonic acid + raffinose experiments (figures 6 and 7), water cannot diffuse to the surface quickly, and it takes approximately 1 hr before any is depleted from the center of the droplet. Nonetheless, the evaporation of water remains significantly faster than that of glycerol, which volatilises only from the outer half of the droplet radius wise.

V. Conclusions

We conclude that the evaporation of small organic components in SOA can be accurately described, within a kinetic multilayer model, by assuming their diffusion follows the Stokes-Einstein relation. The number of evaporation experiments that have been successfully reproduced by KM-GAP, and the range of RHs investigated, give us confidence in this statement. It has also been shown that the practice of optimising model parameters in order to fit diffusion models to experimental data is not required when interpreting experiments of this kind if compositionally dependent viscosities for mixtures can be estimated or measured. The results were reproduced by the KM-GAP model with a small number of physically realistic assumptions, namely: equation (1), Raoult's Law and a mole fraction based mixing rule for viscosity. Therefore, we can say that the simulations described here are predictive rather than postdictive. In this context, the modelling of aerosol properties in which diffusion of semi-volatile organics is important, such as growth rate,[70] surface chemistry,[16] and eventually refractive index,[33] can be simplified.

The apparent volatility of a compound depends strongly on the water content of the particle it is evaporating from: once organic droplets have achieved a sufficient level of drying, the range of observed evaporative fluxes can be explained quantitatively by a path function type dependence of viscosity on composition.

Modelling sequential experiments conducted on the same particle have provided corroborating evidence, since the depletion of semi-volatiles that was predicted to occur in previous steps leads to more accurate simulation of the subsequent evaporation rate. Extrapolating this to atmospheric aerosols, such an effect would manifest most strongly in conditions where organic aerosol undergo glass transitions, namely low temperature and/or RH conditions.[36]

The results of several experiments suggest there may be a set of atmospheric conditions in which the equilibration of SOA with ambient humidity will be thermodynamically controlled, yet the diffusion of organics within the same particles will be kinetically controlled. On the basis of the systems investigated, we believe that the rate of water evaporation can be considered decoupled from organic evaporation in all but the most viscous particles ($>10^{10}$ Pa s).

Supporting Information

The Supporting Information is provided at dx.doi.org/10XX.XXXX.

A list of KM-GAP modifications and parameters; description of the radius retrieval program; a justification for the use of glutaric acid viscosity in place of malonic; description of the time dependent viscosity parametrisation; the mole fractions of malonic acid as a function of water activity (Figure S1); the activity coefficients of malonic acid as a function of water activity (Figure S2); the sensitivity of malonic acid vapour pressure predictions to uncertainties in depletion level and viscosity (Figure S3); the evaporation of malonic acid from a sucrose particle at 20% RH (Figure S4); the refractive indices of the experiments shown in Figure 5 (Figure S5).

Acknowledgements

SI acknowledges funding from GW4+ DTP from NERC(NE/L002434/1). CSD acknowledges funding from the U.S. National Science Foundation (CAREER, AGS-1554936). MS acknowledges funding from the U.S. National Science Foundation (CAREER, AGS-1654104). The authors are grateful to Thomas C. Preston for the sharing of software used in radius fitting, described in the supplement.

References

(1) Shrivastava, M.; Cappa, C. D.; Fan, J.; Goldstein, A. H.; Guenther, A. B.; Jimenez, J. L.; Kuang, C.; Laskin, A.; Martin, S. T.; Ng, N. L.; et al. Recent Advances in Understanding Secondary Organic Aerosol: Implications for Global Climate Forcing. *Rev. Geophys.* **2017**, *55* (2), 509–559.

(2) Glasius, M.; Goldstein, A. H. Recent Discoveries and Future Challenges in Atmospheric Organic Chemistry. *Environ. Sci. Technol.* **2016**, *50* (6), 2754–2764.

(3) Tang, X.; Cocker, D. R.; Asa-Awuku, A. Are Sesquiterpenes a Good Source of Secondary Organic Cloud Condensation Nuclei (CCN)? Revisiting β-Caryophyllene CCN. *Atmos. Chem. Phys.* **2012**, *12* (18), 8377–8388.

(4) Yuan, C.; Ma, Y.; Diao, Y.; Yao, L.; Zhou, Y.; Wang, X.; Zheng, J. CCN Activity of Secondary Aerosols from Terpene Ozonolysis under Atmospheric Relevant Conditions. *J. Geophys. Res. Atmos.* **2017**.

(5) Huang, R.-J.; Zhang, Y.; Bozzetti, C.; Ho, K.-F.; Cao, J.-J.; Han, Y.; Daellenbach, K. R.; Slowik, J.

G.; Platt, S. M.; Canonaco, F.; et al. High Secondary Aerosol Contribution to Particulate Pollution during Haze Events in China. *Nature* **2014**, *514* (7521), 218–222.
(6) Valenzuela, A.; Reid, J. P.; Bzdek, B. R.; Orr-Ewing, A. J. Accuracy Required in Measurements of Refractive Index and Hygroscopic Response to Reduce Uncertainties in Estimates of Aerosol Radiative Forcing Efficiency. *J. Geophys. Res.* **2018**, *123* (12), 6469–6486.
(7) Kanakidou, M.; Seinfeld, J. H.; Pandis, S. N.; Barnes, I.; Dentener, F. J.; Facchini, M. C.; Van Dingenen, R.; Ervens, B.; Nenes, A.; Nielsen, C. J.; et al. Organic Aerosol and Global Climate Modelling: A Review. *Atmos. Chem. Phys.* **2005**, *5*, 1053–1123.
(8) Sato, K.; Fujitani, Y.; Inomata, S.; Morino, Y.; Tanabe, K.; Ramasamy, S.; Hikida, T.; Shimono, A.; Takami, A.; Fushimi, A.; et al. Studying Volatility from Composition, Dilution, and Heating Measurements of Secondary Organic Aerosols Formed during Alpha-Pinene Ozonolysis. *Atmos. Chem. Phys.* **2018**, *18* (8), 5455–5466.
(9) Marshall, F. H.; Berkemeier, T.; Shiraiwa, M.; Ohm, P. B.; Dutcher, S.; Reid, J. P. Influence of Particle Viscosity on Mass Transfer and Heterogeneous Ozonolysis Kinetics in Aqueous – Sucrose – Maleic Acid Aerosol. *Phys. Chem. Chem. Phys.* **2018**, *20*, 15560–15573.
(10) Ingram, S.; Cai, C.; Song, Y.-C.; Glowacki, D. R.; Topping, D. O.; O'Meara, S.; Reid, J. P. Characterising the Evaporation Kinetics of Water and Semi-Volatile Organic Compounds from Viscous Multicomponent Organic Aerosol Particles. *Phys. Chem. Chem. Phys.* **2017**, *19* (47), 31634–31646.
(11) Davies, J. F.; Wilson, K. R. Raman Spectroscopy of Isotopic Water Diffusion in Ultraviscous, Glassy, and Gel States in Aerosol by Use of Optical Tweezers. *Anal. Chem.* **2016**, *88* (4), 2361–2366.
(12) Lienhard, D. M.; Huisman, A. J.; Bones, D. L.; Te, Y.-F.; Luo, B. P.; Krieger, U. K.; Reid, J. P. Retrieving the Translational Diffusion Coefficient of Water from Experiments on Single Levitated Aerosol Droplets. *Phys. Chem. Chem. Phys.* **2014**, *16* (31), 16677.
(13) Krishna, R. Uphill Diffusion in Multicomponent Mixtures. *Chem. Soc. Rev.* **2015**, *44* (10), 2812–2836.
(14) DeRieux, W.-S. W.; Li, Y.; Lin, P.; Laskin, J.; Laskin, A.; Bertram, A. K.; Nizkorodov, S. A.; Shiraiwa, M. Predicting the Glass Transition Temperature and Viscosity of Secondary Organic Material Using Molecular Composition. *Atmos. Chem. Phys.* **2018**, *18* (9), 6331–6351.
(15) Koop, T.; Bookhold, J.; Shiraiwa, M.; Pöschl, U. Glass Transition and Phase State of Organic Compounds: Dependency on Molecular Properties and Implications for Secondary Organic Aerosols in the Atmosphere. *Phys. Chem. Chem. Phys.* **2011**, *13* (43), 19238–19255.
(16) Kurtén, T.; Tiusanen, K.; Roldin, P.; Rissanen, M.; Luy, J.-N.; Boy, M.; Ehn, M.; Donahue, N. α-Pinene Autoxidation Products May Not Have Extremely Low Saturation Vapor Pressures Despite High O:C Ratios. *J. Phys. Chem. A* **2016**, *120* (16), 2569–2582.
(17) Massoli, P.; Lambe, A. T.; Ahern, A. T.; Williams, L. R.; Ehn, M.; Mikkila, J.; Canagaratna, M. R.; Brune, W. H.; Onasch, T. B.; Jayne, J. T.; et al. Relationship between Aerosol Oxidation Level and Hygroscopic Properties of Laboratory Generated Secondary Organic Aerosol (SOA) Particles. *Geophys. Res. Lett.* **2010**, *37*, 5.
(18) Renbaum-Wolff, L.; Grayson, J. W.; Bateman, A. P.; Kuwata, M.; Sellier, M.; Murray, B. J.; Shilling, J. E.; Martin, S. T.; Bertram, A. K. Viscosity of α-Pinene Secondary Organic Material and Implications for Particle Growth and Reactivity. *Proc. Natl. Acad. Sci.* **2013**, *110* (20), 8014–8019.
(19) Song, M.; Liu, P. F.; Hanna, S. J.; Zaveri, R. A.; Potter, K.; You, Y.; Martin, S. T.; Bertram, A. K. Relative Humidity-Dependent Viscosity of Secondary Organic Material from Toluene Photo-Oxidation and Possible Implications for Organic Particulate Matter over Megacities. *Atmos. Chem. Phys.* **2016**, *16* (14), 8817–8830.
(20) Reid, J. P.; Bertram, A. K.; Topping, D. O.; Laskin, A.; Martin, S. T.; Petters, M. D.; Pope, F. D.; Rovelli, G. The Viscosity of Atmospherically Relevant Organic Particles. *Nat. Commun.* **2018**, *9* (1), 956.
(21) Rothfuss, N. E.; Petters, M. D. Characterization of the Temperature and Humidity-Dependent Phase Diagram of Amorphous Nanoscale Organic Aerosols. *Phys. Chem. Chem. Phys.* **2017**, *19* (9), 6532–6545.
(22) Fernandez-Alonso, F.; Bermejo, F. J.; McLain, S. E.; Turner, J. F. C.; Molaison, J. J.; Herwig, K. W. Observation of Fractional Stokes-Einstein Behavior in the Simplest Hydrogen-Bonded Liquid. *Phys. Rev. Lett.* **2007**, *98* (7), 077801.
(23) Saylor, D. M.; Jawahery, S.; Silverstein, J. S.; Forrey, C. Communication: Relationship between Solute Localization and Diffusion in a Dynamically Constrained Polymer System. *J. Chem. Phys.*

2016, *145* (3), 031106.
(24) González, J. A. T.; Longinotti, M. P.; Corti, H. R. Diffusion-Viscosity Decoupling in Supercooled Glycerol Aqueous Solutions. *J. Phys. Chem. B* **2015**, *119* (1), 257–262.
(25) Tarjus, G.; Kivelson, D. Breakdown of the Stokes–Einstein Relation in Supercooled Liquids. *J. Chem. Phys.* **1995**, *103* (8), 3071.
(26) Chen, B.; Sigmund, E. E.; Halperin, W. P. Stokes-Einstein Relation in Supercooled Aqueous Solutions of Glycerol. *Phys. Rev. Lett.* **2006**, *96* (14), 145502.
(27) Mallamace, F.; Branca, C.; Broccio, M.; Corsaro, C.; Gonzalez-Segredo, N.; Spooren, J.; Stanley, H. E.; Chen, S.-H. Transport Properties of Supercooled Confined Water. *Eur. Phys. J. Spec. Top.* **2008**, *161* (1), 19–33.
(28) Douglas, J. F.; Leporini, D. Obstruction Model of the Fractional Stokes ± Einstein Relation in Glass-Forming Liquids. **1998**, *237*, 137–141.
(29) Zobrist, B.; Marcolli, C.; Pedernera, D. A.; Koop, T. Do Atmospheric Aerosols Form Glasses? *Atmos. Chem. Phys.* **2008**, *8* (17), 5221–5244.
(30) Adler, G.; Koop, T.; Haspel, C.; Taraniuk, I.; Moise, T.; Koren, I.; Heiblum, R. H.; Rudich, Y. Formation of Highly Porous Aerosol Particles by Atmospheric Freeze-Drying in Ice Clouds. *Proc. Natl. Acad. Sci.* **2013**, *110* (51), 20414–20419.
(31) Kalberer, M.; Paulsen, D.; Sax, M.; Steinbacher, M.; Dommen, J.; Prevot, A. S. H.; Fisseha, R.; Weingartner, E.; Frankevich, V.; Zenobi, R.; et al. Identification of Polymers as Major Components of Atmospheric Organic Aerosols. *Science* **2004**, *303* (5664), 1659–1662.
(32) Tong, H. J.; Reid, J. P.; Bones, D. L.; Luo, B. P.; Krieger, U. K. Measurements of the Timescales for the Mass Transfer of Water in Glassy Aerosol at Low Relative Humidity and Ambient Temperature. *Atmos. Chem. Phys.* **2011**, *11* (10), 4739–4754.
(33) Song, Y.-C.; Ingram, S.; Arbon, R. E.; Topping, D. O.; Glowacki, D. R.; Reid, J. P. Transient Cavity Dynamics and Divergence from the Stokes–Einstein Equation in Organic Aerosol. *Chem. Sci.* **2020**, *11* (11), 2999–3006.
(34) Hosny, N. A.; Fitzgerald, C.; Vyšniauskas, A.; Athanasiadis, A.; Berkemeier, T.; Uygur, N.; Pöschl, U.; Shiraiwa, M.; Kalberer, M.; Pope, F. D.; et al. Direct Imaging of Changes in Aerosol Particle Viscosity upon Hydration and Chemical Aging. *Chem. Sci.* **2016**, *7* (2), 1357–1367.
(35) Berthier, L.; Biroli, G.; Bouchaud, J.-P.; Cipelletti, L.; Van Saarloos, W. *Dynamical Heterogeneities in Glasses, Colloids, and Granular Media*; Berthier, L., Biroli, G., Bouchaud, J.-P., Cipelletti, L., van Saarloos, W., Eds.; Oxford University Press, 2011.
(36) Maclean, A. M.; Butenhoff, C. L.; Grayson, J. W.; Barsanti, K.; Jimenez, J. L.; Bertram, A. K. Mixing Times of Organic Molecules within Secondary Organic Aerosol Particles: A Global Planetary Boundary Layer Perspective. *Atmos. Chem. Phys.* **2017**, *17* (21), 13037–13048.
(37) Shiraiwa, M.; Li, Y.; Tsimpidi, A. P.; Karydis, V. A.; Berkemeier, T.; Pandis, S. N.; Lelieveld, J.; Koop, T.; Pöschl, U. Global Distribution of Particle Phase State in Atmospheric Secondary Organic Aerosols. *Nat. Commun.* **2017**, *8*, 15002.
(38) Liu, Y.; Wu, Z.; Wang, Y.; Xiao, Y.; Gu, F.; Zheng, J.; Tan, T.; Shang, D.; Wu, Y.; Zeng, L.; et al. Submicrometer Particles Are in the Liquid State during Heavy Haze Episodes in the Urban Atmosphere of Beijing, China. *Environ. Sci. Technol. Lett.* **2017**, *4* (10), 427–432.
(39) Bateman, A. P.; Gong, Z.; Liu, P.; Sato, B.; Cirino, G.; Zhang, Y.; Artaxo, P.; Bertram, A. K.; Manzi, A. O.; Rizzo, L. V.; et al. Sub-Micrometre Particulate Matter Is Primarily in Liquid Form over Amazon Rainforest. *Nat. Geosci.* **2015**, *9* (1), 34–37.
(40) Ullmann, D. A.; Hinks, M. L.; Maclean, A.; Butenhoff, C.; Grayson, J.; Barsanti, K.; Jimenez, J. L.; Nizkorodov, S. A.; Kamal, S.; Bertram, A. K. Viscosities, Diffusion Coefficients, and Mixing Times of Intrinsic Fluorescent Organic Molecules in Brown Limonene Secondary Organic Aerosol and Tests of the Stokes-Einstein Equation. *Atmos. Chem. Phys.* **2019**, *19*, 149–1503.
(41) Yli-Juuti, T.; Pajunoja, A.; Tikkanen, O. P.; Buchholz, A.; Faiola, C.; Vaisanen, O.; Hao, L.; Kari, E.; Perakyla, O.; Garmash, O.; et al. Factors Controlling the Evaporation of Secondary Organic Aerosol from Alpha-Pinene Ozonolysis. *Geophys Res Lett* **2017**, *44* (5), 2562–2570.
(42) Song, Y. C.; Haddrell, A. E.; Bzdek, B. R.; Reid, J. P.; Bannan, T.; Topping, D. O.; Percival, C.; Cai, C. Measurements and Predictions of Binary Component Aerosol Particle Viscosity. *J. Phys. Chem. A* **2016**, *120* (41), 8123–8137.
(43) Rickards, A. M. J.; Song, Y.-C.; Miles, R. E. H.; Preston, T. C.; Reid, J. P. Variabilities and Uncertainties in Characterising Water Transport Kinetics in Glassy and Ultraviscous Aerosol. *Phys. Chem. Chem. Phys.* **2015**, *17* (15), 10059–10073.

(44) Becker, S. R.; Poole, P. H.; Starr, F. W. Fractional Stokes-Einstein and Debye-Stokes-Einstein Relations in a Network-Forming Liquid. *Phys. Rev. Lett.* **2006**, *97* (5), 055901.
(45) Price, H. C.; Mattsson, J.; Murray, B. J. Sucrose Diffusion in Aqueous Solution. *Phys. Chem. Chem. Phys.* **2016**, *18* (28), 19207–19216.
(46) Evoy, E.; Maclean, A. M.; Rovelli, G.; Li, Y.; Tsimpidi, A. P.; Karydis, V. A.; Kamal, S.; Lelieveld, J.; Shiraiwa, M.; Reid, J. P.; et al. Predictions of Diffusion Rates of Large Organic Molecules in Secondary Organic Aerosols Using the Stokes–Einstein and Fractional Stokes–Einstein Relations. *Atmos. Chem. Phys.* **2019**, *19* (15), 10073–10085.
(47) Mitchem, L.; Reid, J. P. Optical Manipulation and Characterisation of Aerosol Particles Using a Single-Beam Gradient Force Optical Trap. *Chem. Soc. Rev.* **2008**, *37* (4), 756.
(48) Cai, C.; Stewart, D. J.; Preston, T. C.; Walker, J. S.; Zhang, Y. H.; Reid, J. P. A New Approach to Determine Vapour Pressures and Hygroscopicities of Aqueous Aerosols Containing Semi-Volatile Organic Compounds. *Phys. Chem. Chem. Phys.* **2014**, *16* (7), 3162–3172.
(49) Rovelli, G.; Miles, R. E. H.; Reid, J. P.; Clegg, S. L. Accurate Measurements of Aerosol Hygroscopic Growth over a Wide Range in Relative Humidity. *J. Phys. Chem. A* **2016**, *120* (25), 4376–4388.
(50) Glantschnig, W. J.; Chen, S.-H. Light Scattering from Water Droplets in the Geometrical Optics Approximation. *Appl. Opt.* **1981**, *20* (14), 2499–2509.
(51) Shiraiwa, M.; Pfrang, C.; Koop, T.; Pöschl, U. Kinetic Multi-Layer Model of Gas-Particle Interactions in Aerosols and Clouds (KM-GAP): Linking Condensation, Evaporation and Chemical Reactions of Organics, Oxidants and Water. *Atmos. Chem. Phys.* **2012**, *12* (5), 2777–2794.
(52) Mai, H.; Shiraiwa, M.; Flagan, R. C.; Seinfeld, J. H. Under What Conditions Can Equilibrium Gas–Particle Partitioning Be Expected to Hold in the Atmosphere? *Environ. Sci. Technol.* **2015**, *49* (19), 11485–11491.
(53) Berkemeier, T.; Ammann, M.; Krieger, U. K.; Peter, T.; Spichtinger, P.; Pöschl, U.; Shiraiwa, M.; Huisman, A. J. Technical Note: Monte-Carlo Genetic Algorithm (MCGA) for Model Analysis of Multiphase Chemical Kinetics to Determine Transport and Reaction Rate Coefficients Using Multiple Experimental Data Sets. *Atmos. Chem. Phys.* **2017**, *17*, 8021–8029.
(54) Cai, C.; Miles, R. E. H.; Cotterell, M. I.; Marsh, A.; Rovelli, G.; Rickards, A. M. J.; Zhang, Y.; Reid, J. P. Comparison of Methods for Predicting the Compositional Dependence of the Density and Refractive Index of Organic–Aqueous Aerosols. *J. Phys. Chem. A* **2016**, *120* (33), 6604–6617.
(55) Nandy, L.; Ohm, P. B.; Dutcher, C. S. Isotherm-Based Thermodynamic Models for Solute Activities of Organic Acids with Consideration of Partial Dissociation. *J. Phys. Chem. A* **2016**, *120* (24), 4147–4154.
(56) Dutcher, C. S.; Ge, X.; Wexler, A. S.; Clegg, S. L. An Isotherm-Based Thermodynamic Model of Multicomponent Aqueous Solutions, Applicable Over the Entire Concentration Range. *J. Phys. Chem. A* **2013**, *117* (15), 3198–3213.
(57) Ohm, P. B.; Asato, C.; Wexler, A. S.; Dutcher, C. S. Isotherm-Based Thermodynamic Model for Electrolyte and Nonelectrolyte Solutions Incorporating Long- and Short-Range Electrostatic Interactions. *J. Phys. Chem. A* **2015**, *119* (13), 3244–3252.
(58) Bzdek, B. R.; Power, R. M.; Simpson, S. H.; Reid, J. P.; Royall, P. Precise, Contactless Measurements of the Surface Tension of Picolitre Aerosol Droplets. *Chem. Sci.* **2015**.
(59) Gervasi, N. R.; Topping, D. O.; Zuend, A. A Predictive Group-Contribution Model for the Viscosity of Aqueous Organic Aerosol. *Atmos. Chem. Phys.* **2020**, *20* (5), 2987–3008.
(60) Rovelli, G.; Song, Y.-C.; Maclean, A. M.; Topping, D. O.; Bertram, A. K.; Reid, J. P. Comparison of Approaches for Measuring and Predicting the Viscosity of Ternary Component Aerosol Particles. *Anal. Chem.* **2019**, *91* (8), 5074–5082.
(61) Vander Wall, A. C.; Lakey, P. S. J.; Rossich Molina, E.; Perraud, V.; Wingen, L. M.; Xu, J.; Soulsby, D.; Gerber, R. B.; Shiraiwa, M.; Finlayson-Pitts, B. J. Understanding Interactions of Organic Nitrates with the Surface and Bulk of Organic Films: Implications for Particle Growth in the Atmosphere. *Environ. Sci. Process. Impacts* **2018**, *20* (11), 1593–1610.
(62) Petters, M. D.; Kreidenweis, S. M. A Single Parameter Representation of Hygroscopic Growth and Cloud Condensation Nucleus Activity. *Atmos. Chem. Phys.* **2007**, *7* (8), 1961–1971.
(63) Rickards, A. M. J.; Miles, R. E. H.; Davies, J. F.; Marshall, F. H.; Reid, J. P. Measurements of the Sensitivity of Aerosol Hygroscopicity and the κ Parameter to the O/C Ratio. *J. Phys. Chem. A* **2013**, *117* (51), 14120–14131.
(64) Soonsin, V.; Zardini, A. A.; Marcolli, C.; Zuend, A.; Krieger, U. K. The Vapor Pressures and Activities of Dicarboxylic Acids Reconsidered: The Impact of the Physical State of the Aerosol.

Atmos. Chem. Phys. **2010**, *10* (23), 11753–11767.

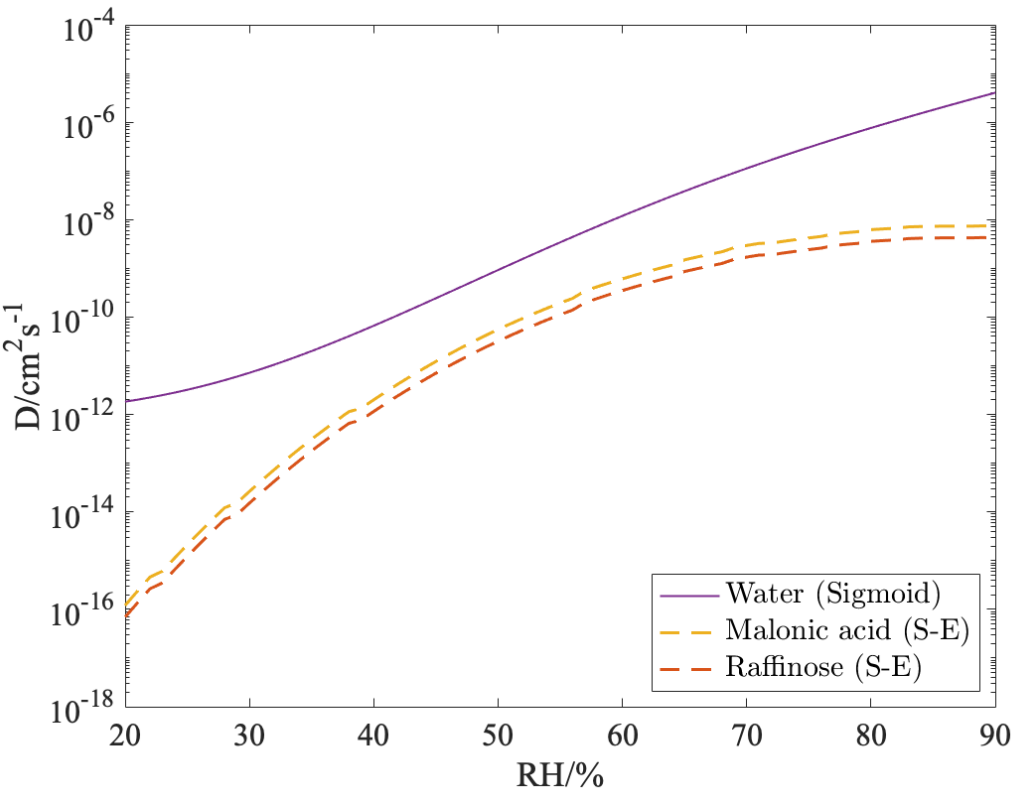

Figure 1: Composition dependent diffusion coefficients of the components of ternary aerosol droplets investigated in this work. Water (purple line) is represented by a sigmoidal parametrisation fit in our previous publication.[10] Raffinose and malonic acid (red and orange dashed respectively) are determined using equation 1, assuming a 3:2 molar ratio in conjunction with viscosity data from Song et. al 2016.[42]

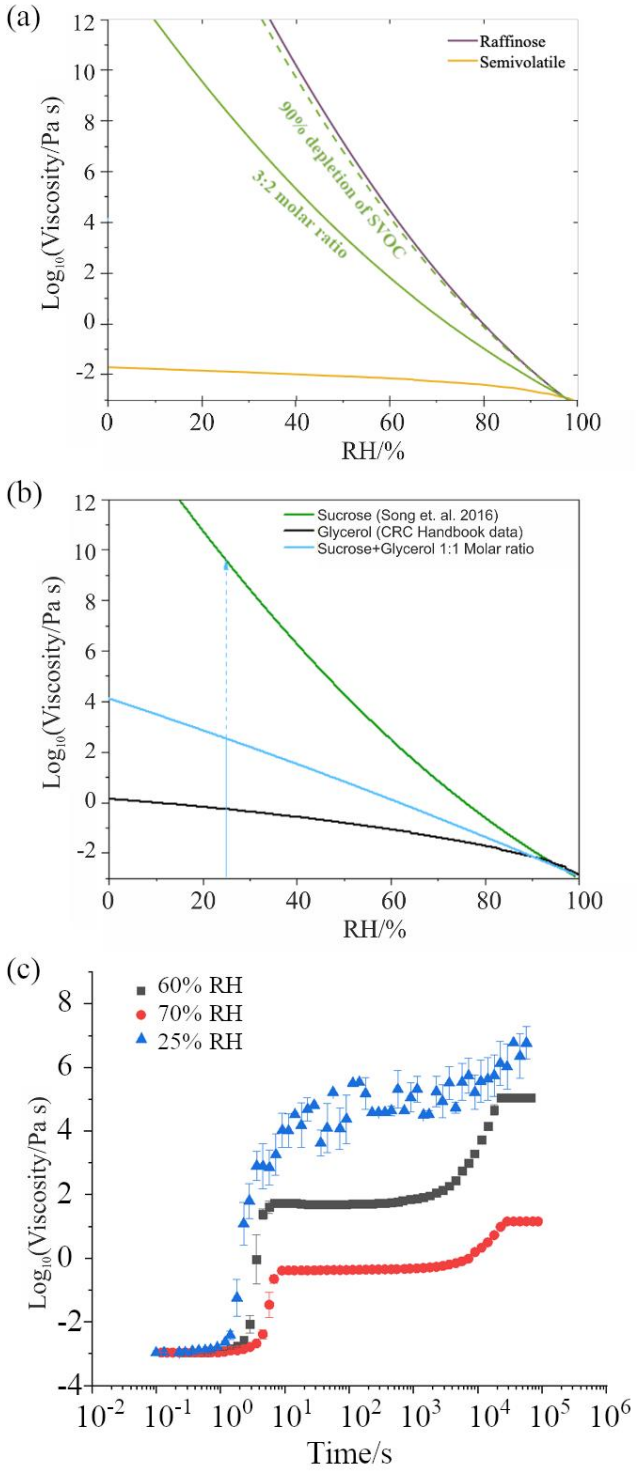

Figure 2: Viscosity parametrisations of ternary particles investigated in this work, showing increasing complexity. (a) Mole fraction weighted mixing rule predicting the viscosity of particles containing raffinose (purple) and a semi-volatile organic compound (glutaric acid, yellow). (b) Bosse mixing rule (see main text) predicting the viscosity of particles containing sucrose (green) and glycerol (black), taking into account the differing hygroscopic properties of the two compounds. The vertical line indicates the RH at which the experiment described in section IV.c was conducted. (c) A time dependent Bosse mixing predicting the viscosity of particles containing sucrose and glycerol at three RHs, using compositions determined from the optical properties.

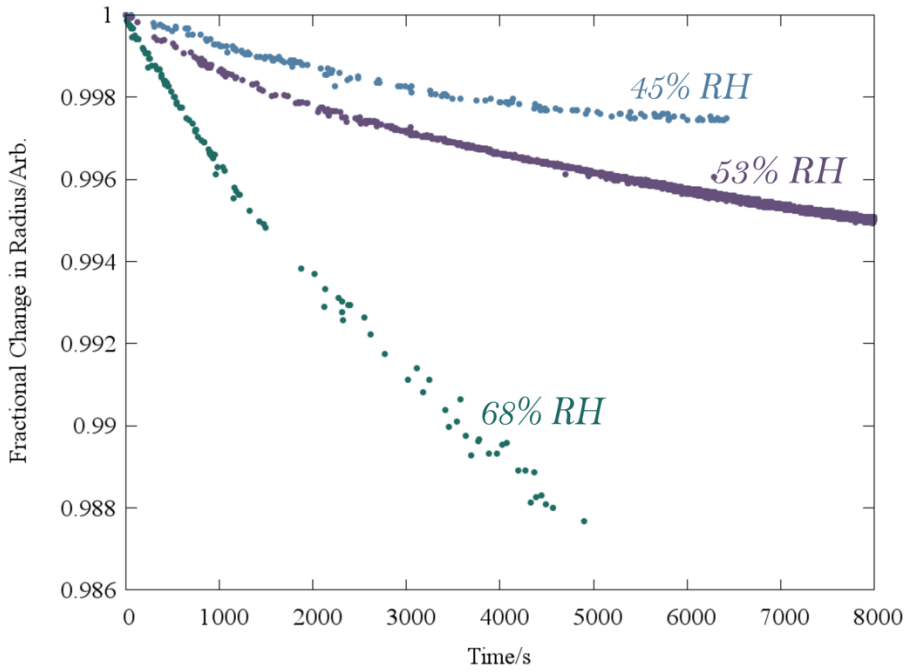

Figure 3: Comparison of the relative changes in particle radius due to malonic acid evaporation from optically tweezed raffinose particles. Decreased intraparticle diffusion causes slower evaporation as the humidity is lowered – from 45% (blue points) to 53% (purple points) to 68% (dark green points). Each curve is normalised to its initial radius.

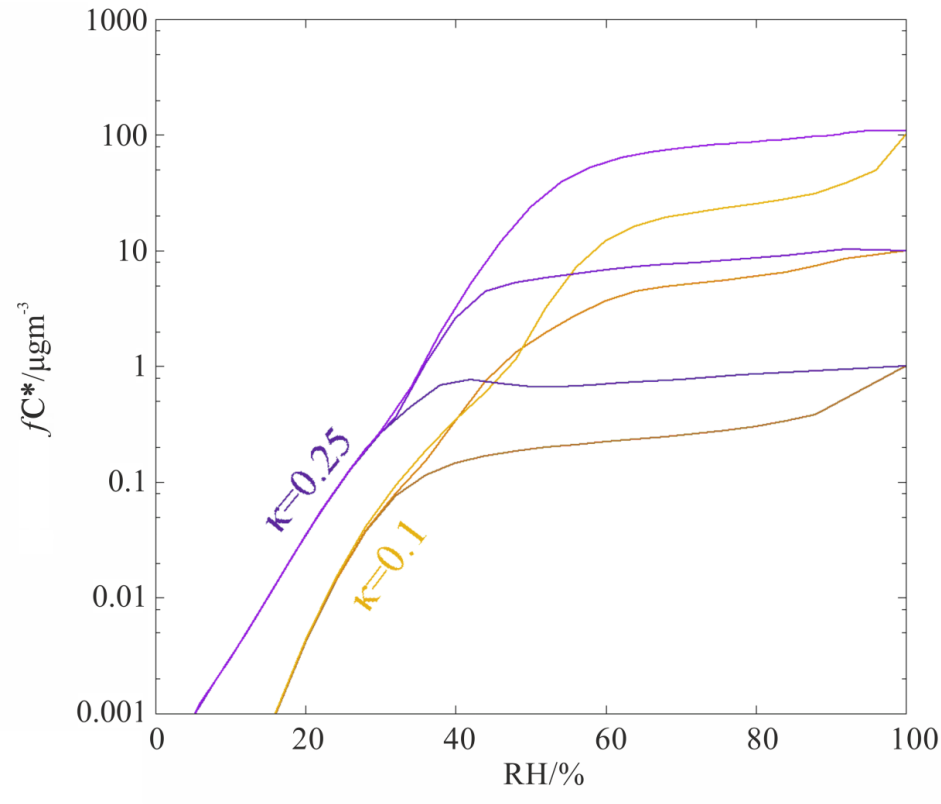

Figure 4: The modelled impact of humidity on mass loading of SVOC molecules evaporating from a 200 nm particle. Viscosity is taken from a log-linear representation of toluene SOA from Song et. al.[19] The un-supressed volatilities of the compounds were defined to correspond to mass loadings of 100, 10, and 1 μg m^{-3} (top to bottom respectively). Note that the simulations converge to each of these values at RH = 100%.

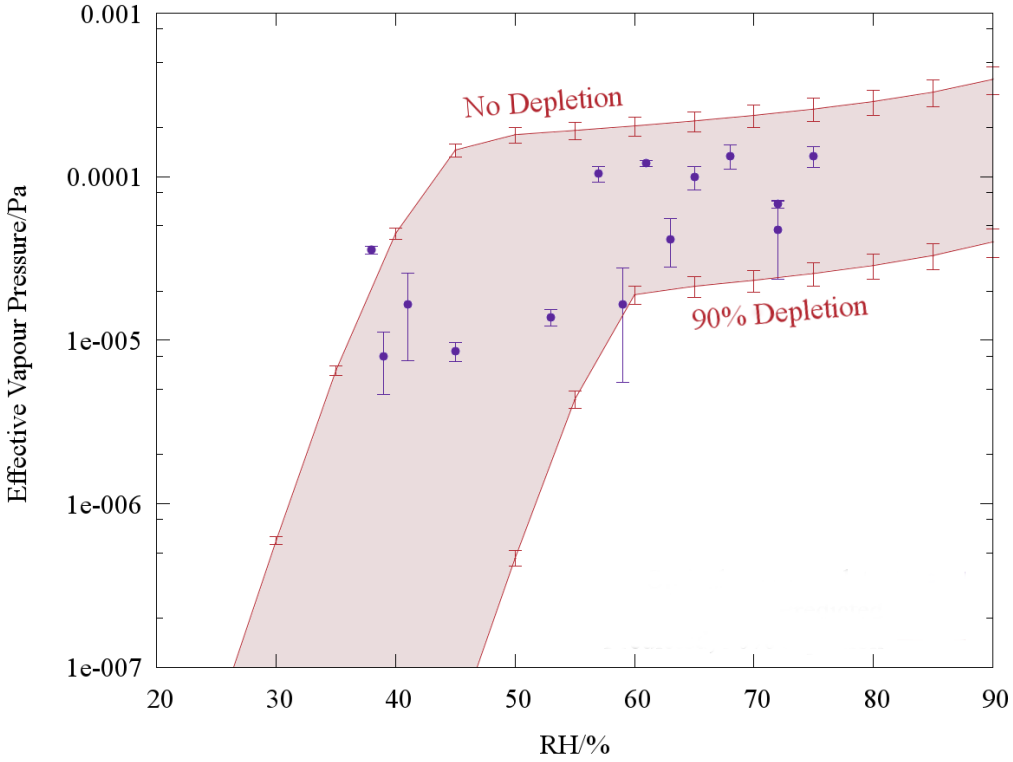

Figure 5: Comparison of observed (blue points) and predicted (red points and envelope) effective pure component vapour pressures of malonic acid evaporation from raffinose droplets. The envelope is bounded by two KM-GAP simulations, beginning from extremes in starting composition.

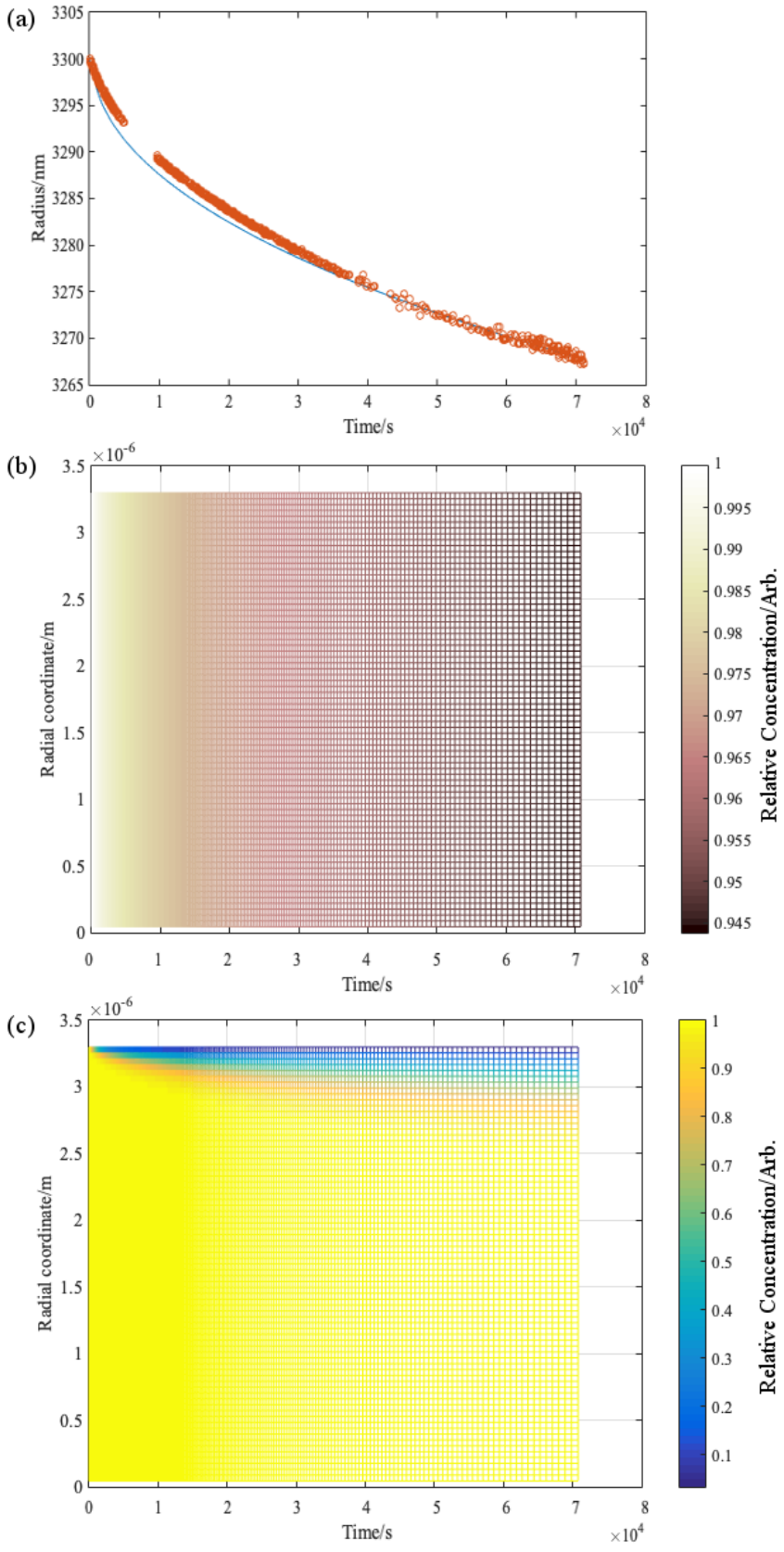

Figure 6: (a) **:** KM-GAP prediction of the radius change (blue line) due to evaporation of malonic acid from a raffinose particle at 53% RH. Bulk concentration profiles of (b) water and (c) malonic acid are also presented (see main text for description of how they are calculated).

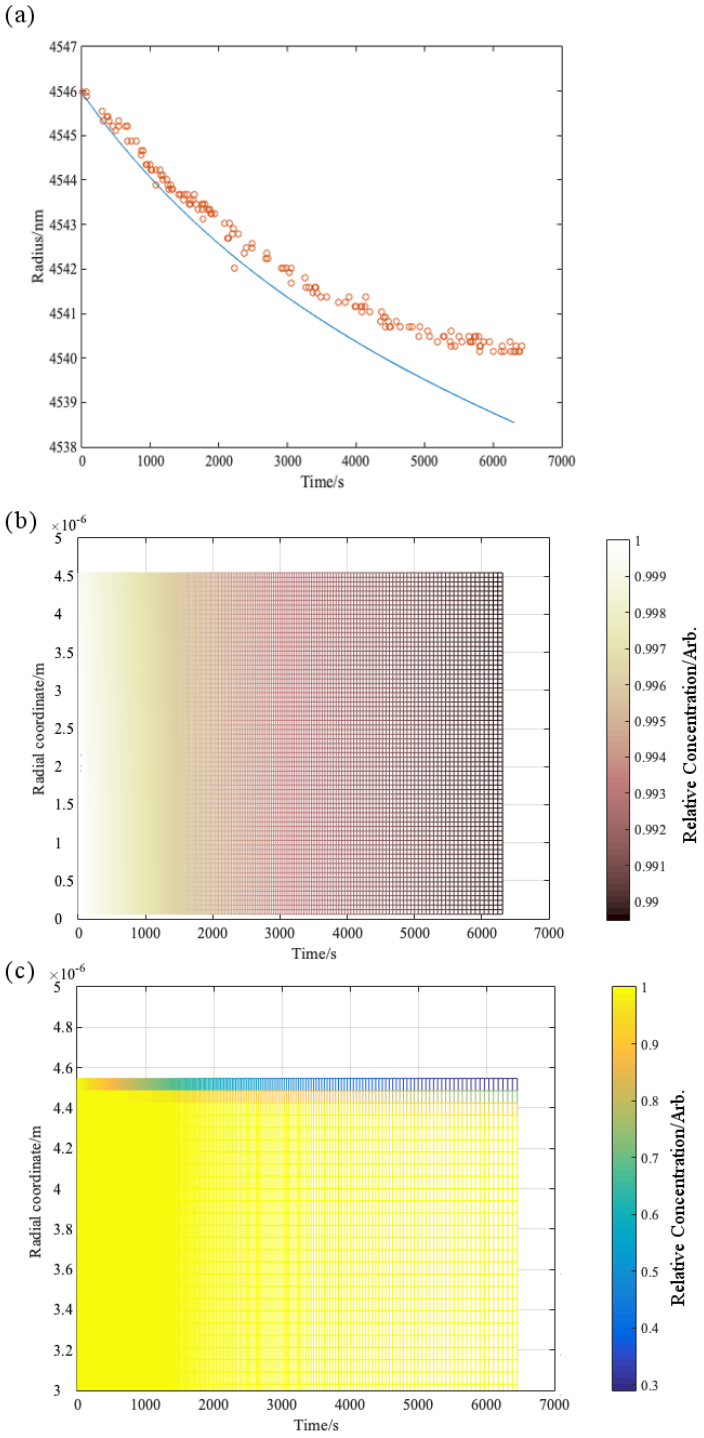

Figure 7: (a) KM-GAP prediction of the radius change (blue line) due to evaporation of malonic acid from raffinose particles at 45% RH. Bulk concentration gradients of (b) water and (c) malonic acid are also presented (see main text for description of how they are calculated). Note that the y axis in panel (c) has been zoomed in, in contrast to 7c.

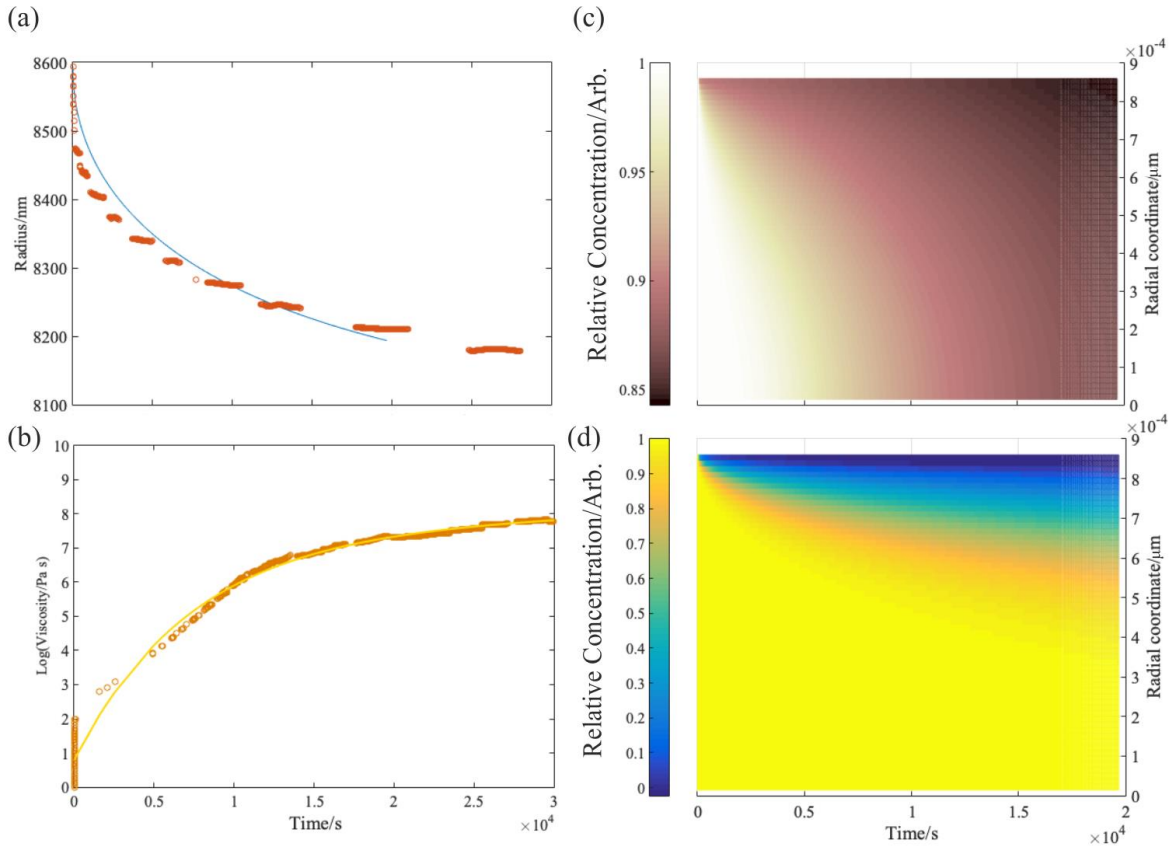

Figure 8: (a) Comparison of KM-GAP predictions of the radius change (blue line) due to evaporation of glycerol from a sucrose particles at 25% RH with electrodynamic balance data (orange points). (b) Time dependent viscosity over the same interval: The Bosse treatment of sucrose and glycerol (orange points) was converted into a smooth function bi-exponential fit (yellow curve) before inclusion in the model simulation. Bulk concentration gradients of (c) water and (d) glycerol are also presented.

For Table of Contents Only: